Dynamic Spallation in Uranium under Laser Shock Loading *

Da-Wu Xiao(肖大武)[1], Hua Shu(舒桦)[2], Dong-Li Zou(邹东利)[1], Chao Lu(路超)[1], Li-Feng He(何立峰)[1]**

[1]*Institute of Materials, China Academy of Engineering Physics, Mianyang 621700*
[2]*Institute of Laser, China Academy of Engineering Physics, Mianyang 621907*

(Received 18 September 2018)

The spall behavior of uranium is investigated using direct laser ablation loading experiments. The uranium targets are cut and ground to 0.05 mm, 0.1 mm, and 0.15 mm in thickness. Laser energies are varied to yield a constant peak pressure. This results in different strain rates and varying degrees of damage to the uranium targets. The spall strength is calculated and analyzed from the free surface velocity histories recorded using a line velocity interferometer for any reflections system. The spall strength increases from 4.3 GPa to 9.4 GPa with strain rates ranging from $4.0 \times 10^6\,s^{-1}$ *to* $1.7 \times 10^7\,s^{-1}$. *Post-mortem analysis is performed on the recovered samples, revealing the twin-matrix interfaces together with the inclusions to be the primary factor governing the spall fracture of uranium.*

PACS: 62.50.−p, 62.50.Ef, 62.20.mm DOI: 10.1088/0256-307X/36/2/026201

Uranium is widely used in nuclear and non-nuclear applications as radiation shields or kinetic energy penetrators. Previous studies of spallation in uranium have shown a dependence of spall behaviors on alloy solute concentration, grain size, content of inclusion, and strain rate.[1−4] For uranium alloys, the spall strength is higher than that of pure uranium under similar loading conditions. Zurek *et al.*[5] and Hixson *et al.*[6] investigated spall behavior of uranium targets with different carbide inclusion contents by plate impact experiments, and the results show that the spall strengths of both the 38 ppm C uranium target and 280 ppm C uranium target were 1.9 GPa. Meanwhile, the fracture modes were different, there was a transgranular fracture for 280 ppm C uranium target and intergranular fracture for 38 ppm C uranium target. Grady[7] reported that the spall strengths of uranium were 2.6 GPa–3.3 GPa under shock pressure ranging from 3 GPa to 15 GPa, and the corresponding strain rates ranged from $2.7 \times 10^5\,s^{-1}$ to $4.1 \times 10^6\,s^{-1}$. Cochran and Banner[8] reported a spall strength of 2.4 GPa for the fine grain size uranium targets (about 10 μm) by gas gun experiments with a shock pressure 4 GPa and less. Robbins *et al.*[1,9] also reported the spall behavior of uranium targets with two different purities by laser-driven flyer spall experiments. The spall strengths of high purity uranium and low purity uranium were 4.4 GPa and 2.9 GPa at a strain rate of $10^6\,s^{-1}$, respectively. A few reports of metallurgical examinations for the recovered uranium spall debris have been presented. However, these qualitative descriptions of dynamic failure leave many unanswered questions, including the mechanism of microvoid nucleation in uranium. Consequently, this work was undertaken to attempt to obtain a better micro-mechanical understanding of spallation in uranium, which may help greatly in modeling spall processes.

Depleted uranium foils containing 80 wppm carbon were used in these experiments. The targets were cut from cast stock with a low speed abrasive wheel and they were ground to thicknesses of 0.05 mm, 0.10 mm or 0.15 mm, and were then briefly polished to remove the oxide layer and measured for thickness before loading in the capsules. The polishing time is preferably within 3 min to avoid the residual stress. Immediately after the preparation, the capsule is evacuated (better than 10^{-2} Pa) to avoid surface oxidation. Shock waves were generated in the uranium foils by direct laser ablation loading, using the ninth beam of Shenguang-Ⅱ Nd:glass laser facility at the National Laboratory on High Power Laser and Physics. This laser delivered pulses of light at $\lambda = 351$ nm with energies up to 3.0 kJ, and the temporal profile of the laser is nearly square with a rise and fall time of ∼300 ps and a full width at half maximum (FWHM) of ∼2.4 ns. The laser beam was smoothed using a lens-array system to eliminate large-scale spatial modulation and to obtain a flat-topped profile in the focal plane. The absorbed laser intensity of the focal spot was $\sim 10^{15}\,W/cm^2$ with a flat region of 1.0 mm×0.7 mm. To monitor the process of spall fracture, the time-resolved free surface velocity profiles of the shocked sample were measured with a line velocity interferometer to find any reflections in the (VISAR) system. The VISAR system had a temporal resolution of ∼20 ps and a spatial resolution of ∼7 μm.

After impact, a metallographic analysis was carried out on the spalled and incipiently spalled samples. The fine structure of impacted region was examined with scanning electron microscopy (SEM) and electron backscattered diffraction (EBSD) observations with a Helios Nanolab 600i operated at 25 kV. The specimens were prepared for EBSD observation using

*Supported by the Science Foundation of China Academy of Engineering Physics under Grant No A090504.
**Corresponding author. Email: hopkinson@163.com
© 2019 Chinese Physical Society and IOP Publishing Ltd

a two-step electro-polish procedure reported in detail in Ref. [10]. Automated EBSD scans were performed using a TSL camera attached to a dual beam FIB (FEI Helios NanoLab DualBeam system) at a voltage of 25 kV with a 1 μm step size using TSL OIM^{TM1} Data Collection software. EBSD crystal orientation results were analyzed with TSL OIM^{TM} analysis software.

A typical line VISAR image of the experiment is shown in Fig. 1(a). Distance is represented in the vertical direction of the image, with the time in the horizontal direction. The temporal scale of the image is 50 ns. The length of the etalon is 60 mm corresponding to the fringe constant of 900 m/s/fringe. The flat shock breakout can be observed as a rapid shift of fringes across the interferogram, followed by a slower return of the fringes during the material pullback. To obtain the phase as a function of time, lineouts were taken along the time axis, Fourier transformed, and spectrally filtered to include only the positive frequency information and inverse Fourier transform. Figure 1(b) shows the free surface velocity profile of a uranium foil of 148 μm thickness with the drive laser energy about 327 J at the wavelength of 2ω. By extracting the maximum and minimum velocities. the 'pull-back' velocity Δu is obtained from the free surface velocity profile of the target rear surface. The difference in the corresponding times of these velocities, Δt, is used to calculate the tensile strain rate for each impact

$$\dot{\varepsilon} = \frac{\Delta u}{\Delta t}\frac{1}{2C_{\rm b}}, \tag{1}$$

the spall strength $\sigma_{\rm s}$ could be estimated using

$$\sigma_{\rm s} = \frac{1}{2}\rho_0 C_{\rm b}\Delta u, \tag{2}$$

where the material density ρ_0 (19.0±1 g/cm^3) for uranium was measured using the Archimedes technique, and the bulk speed of sound $C_{\rm b}$ (2.393±3 km/s) was obtained by the resonant ultrasound spectroscopy (RUS) technique.

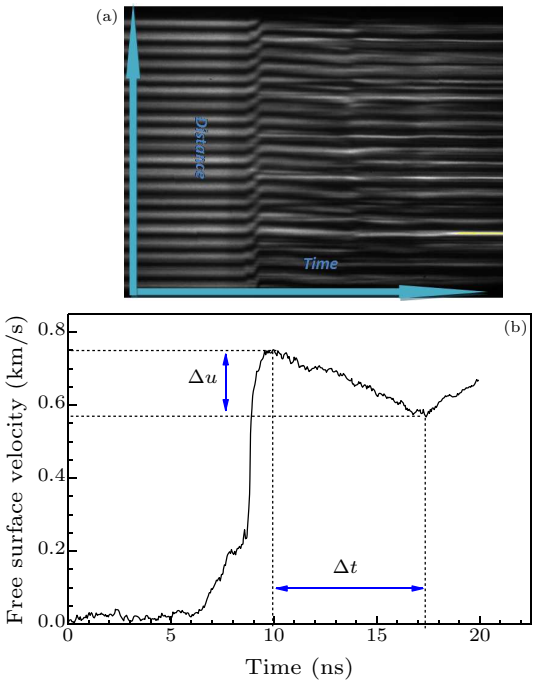

Fig. 1. Experimental results of uranium targets by direct laser ablation: (a) typical line VISAR diagnostics, (b) subsequent velocity-time response 148 μm thickness target with drive laser energy of 327 J.

Table 1 summarizes the parameters of laser impact loading and the principal results of the experiments. The laser incident intensity was calculated by laser energy and focal area. According to data of the incident intensity $I_{\rm L}$ and wavelength ($\lambda = 0.351$ μm) of the laser, the peak shock pressure in the sample can be calculated by $P = 4000(I_{\rm L}/\lambda)^{2/3}$ GPa.[11] Target thicknesses and corresponding laser intensities were chosen to access different strain rates at the spall plane while roughly maintaining the same peak shock pressure about 500 GPa.

Table 1. Experimental parameters and results.

Target	Thickness(μm)	$I_{\rm L}$ (10^{15} W/cm^2)	P (GPa)	Δt(ns)	Δu (m/s)	$\dot{\varepsilon}$ (10^6 s^{-1})	$\sigma_{\rm s}$ (GPa)
1	50	0.320	492	5.0±0.2	334±4	14	7.6
2	50	0.210	589	5.0±0.3	413±4	17	9.4
3	93	0.381	552	9.3±0.4	334±3	7.5	7.6
4	100	0.327	500	12.8±0.4	246±2	4.0	5.6
5	148	0.612	578	8.0±0.4	189±2	4.9	4.3

The spall strength of uranium measured in this study is compared with that of previous reports as shown in Fig. 2. The most striking trend is the significantly greater spall strength by laser shock loading relative to that measured with gas gun by other investigators, and the spall strength increases much faster with increasing the strain rate. The spallation process of materials is influenced by many factors, such as preparation process, microstructure, initial temperature and loading strain rate. The spall strength for strain rates higher than 10^5 s^{-1} presents an exponential increasing tendency up to the ultimate tensile strength.[12–15] This higher spall strength is suggestive of a strong time dependence of the phenomenon, consistent with the nucleation and growth kinetics of voids and the strain rate sensitivity embedded in the Grady theory.[16] The relation between strain rates and spall strength can be expressed as

$$\sigma_{\rm s} = (3\rho_0 C_{\rm b} K_{\rm c}^2 \dot{\varepsilon})^m, \tag{3}$$

where the fracture toughness for uranium is $K_{\rm c} = 60\,{\rm MPa\cdot m^{1/2}}$, and $m = 0.28$ represents the strain rate

dependence. The calculated theoretical curve in Fig. 2 is in reasonable agreement with the experimental data.

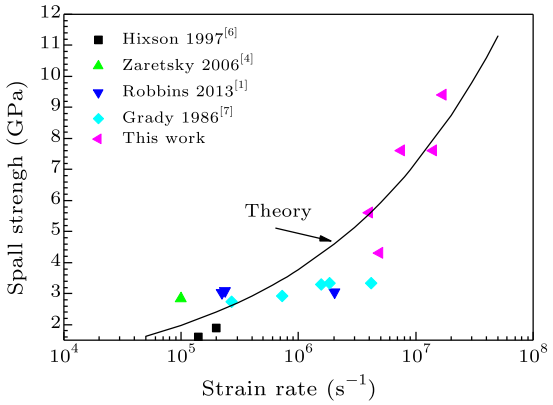

Fig. 2. Relations between spall strength and strain rate for uranium.

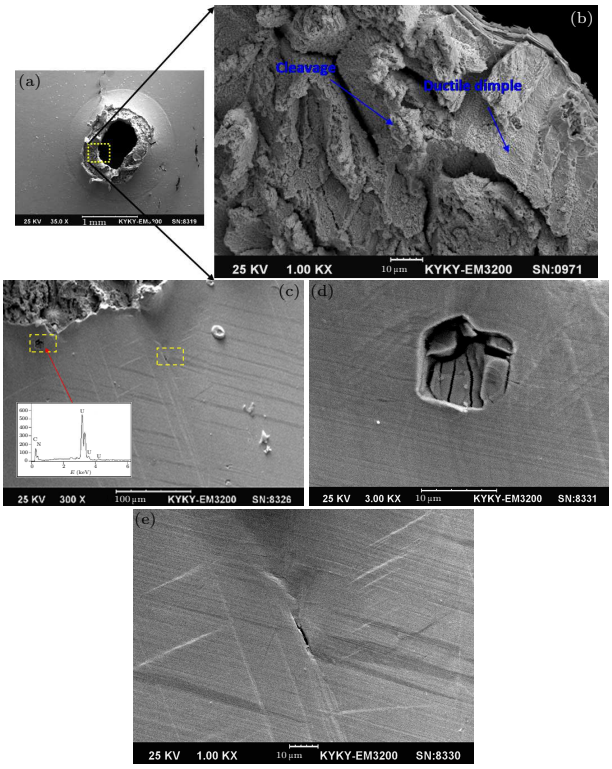

Fig. 3. Scanning-electron microscope image showing the exposed spall plane of (a) target 4, (b) highly magnified microstructure of fracture surface, (c) enlarged details of the edge of the impact zone, (d)cracked inclusions, and (e) a microcrack along twin-matrix interface.

The surface morphologies of the spall failure surfaces were imaged using SEM. Figures 3(a) and 3(b) show the failure surface of target 4, for which the fracture contour coincides with the size of the focal spot. The highly magnified microstructures of fracture surface shown in Figs. 3(a) and 3(b) exhibit a mixed-mode failure, consisting of predominantly brittle intergranular fracture with regions of ductile dimpling. A similar fracture was previously observed by Zurek.[5] In Fig. 3(c), high density of acicular twinning structures were observed in the edge of the impact zone. Impurities have very low solubility in uranium, and they usually form second phase particles that may decrease macroscopic ductility. Carbon forms carbide inclusions, which may decrease ductility in a manner similar to carbides in ferritic steels. As shown in Fig. 3(d). the UC inclusion cracked in the process of impact. Moreover, the hydrostatic tension in the spall test is expected to facilitate the microcrack nucleation. The sample is subjected to extremely high strain rate and very high pressure deformation during the course of laser ablation shock loading, which makes the accommodation of plastic deformation at a crack tip more difficult and therefore favor intergranular or transgranular brittle fracture. The spall process involves the activation and growth of mature ductile cracks before coalescence and spall failure occurs. This deformation usually generates a very high density of dislocations. In the case of uranium, a large number of deformation twins, and also twin intersections and twin-matrix interfaces can serve as preferred nucleation sites for sharp brittle cracks. Figure 3(e) shows a microcrack generated along the twin-matrix interface on the target-4 rear surface.

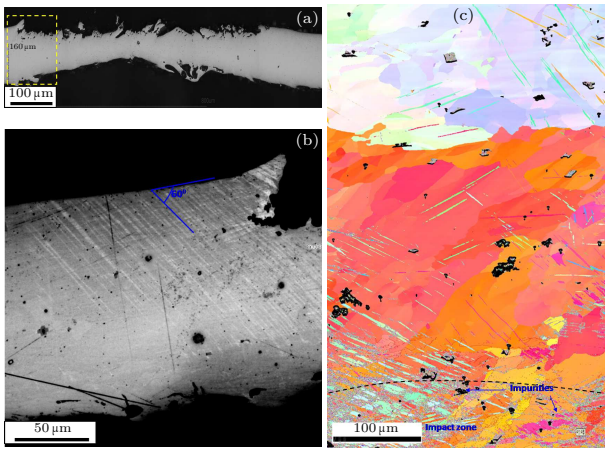

Fig. 4. The metallurgical structure of incipiently spalled target 5: (a) cross section, (b) enlarged details of edge of impact zone, and (c) the inverse pole figure map of transverse section.

Metallographic samples, cutting through the center of the spalled sample (target 4) in direction parallel to the loading direction, were prepared for optical micrography analysis. Figures 4(a) and 4(b) show the metallurgical structure of cross sections of the recovered spalled target 5. The spall region is clearly visible in these images as the region exhibits uneven fracture. A large number of acicular twinning structures were observed in the enlarged details of edge of impact zone in the direction of 60° along the loading axis, and the distance of twinning lamella was about 1–2 μm. Figure 4(c) shows the inverse pole figure map of transverse section of the recovered spalled target 5, and the black spots in the figure represent the impurities. It is important to note that the impurity concentration over large target areas is not homogeneous, as shown in Fig. 4(c). This figure shows that in the impact zone of the target where impurity preferen-

tially clusters have a relatively higher twinning density than that of the matrix. This observation seems to be consistent with the idea that the inclusions together with the twin-matrix interfaces to be preferred sites for growth of cracks in uranium.

In summary, impact loading of a uranium sample was applied by direct laser ablation. The spall strength increases rapidly from 4.3 GPa to 9.4 GPa with an increase in the strain rate. The recovered samples were carefully analyzed with fracture surface morphology and metallurgical graphy, which reveal that the brittle impurities, particularly twinning in the specimen, not only precede failure but are also likely to be micromechanical factors in the very generation of the spallation for uranium.

We gratefully acknowledge the valuable support for the experiments by the Shenguang-Ⅱ technical crews.

References

[1] Robbins D L and Sheffield S A 2013 *LA-UR* 0962
[2] Kozlov E A, Bondarchuk S V, Zuev Y N et al 2011 *Phys. Met. Metallogr.* **111** 410
[3] Kozlov E A, Pankratov D G, Taranov V I et al 2009 *Phys. Met. Metallogr.* **108** 401
[4] Zaretsky E, Herrmann B and Shrarts D 2006 *Pflügers Arch. - Eur. J. Physiol.* **134** 971
[5] Zurek A K, Embury J D, Kelly A et al 1997 *SCCM AIP Conf Proc.* **429** 423
[6] Hixson R S, Vorthman J E, Gustavsen R L et al 1997 *SCCM AIP Conf Proc.* **429** 479
[7] Grady D E 1986 *Metallurgical Applications of Shock-Wave and High-Strain-Rate Phenomena* (New York: Marcel Dekker) p 763
[8] Cochran S and Banner D 1977 *J. Appl. Phys.* **48** 2729
[9] Robbins D L, Kelly A M, Alexander D J et al 2001 *SCCM AIP Conf Proc.* **620** 499
[10] Mccabe R J and Teter D F 2006 *J. Microsc.* **223** 33
[11] Phipps C R 1988 *J. Appl. Phys.* **64** 1083
[12] Pedrazas N A, Worthington D L, Dalton D A, Sherek P A, Steuck S P, Quevedo H J, Bernstein A C, Taleff E M and Ditmire T 2012 *Mater. Sci. Eng. A* **536** 117
[13] Cuq-Lelandais J P, Boustie M, Soulard L, Berthe L et al 2010 *EPJ. Web Conf.* **10** 00014
[14] Moshe E, Eliezer S, Dekel E et al 1998 *J. Appl. Phys.* **83** 8
[15] Remington T P, Hahn E N, Zhao S et al 2018 *Acta Mater.* **158** 313
[16] Grady D E 1988 *J. Mech. Phys. Solids* **36** 353